Thesis Title

A subtitle of your thesis

Author name

Thesis submitted for the degree of
Master in Master's Program Name <change at main.tex>
60 credits

Department Name <change at main.tex>
Faculty name <change in duoforside.tex>

UNIVERSITY OF OSLO

Spring 2022

Thesis Title

A subtitle of your thesis

Author name

Thesis Title

http://www.duo.uio.no/

Printed: Reprosentralen, University of Oslo

Abstract

Contents

List of Figures

List of Tables

Preface

Chapter 1

Introduction

some introduction on the importance of discovering new materials and alloying.
Need something on thermoelectricity related to both the band gap and high-entropy alloys.

High-entropy alloys is a novel class of materials based on alloying multiple components, as opposed to the more traditional binary alloys. This results in an unprecedented opportunity for discovery of new materials with a superior degree of tuning for specific properties and applications. Recent research on high-entropy alloys have resulted in materials with exceedingly strong mechanical properties such as strength, corrosion and temperature resistance, etc **find references**. Meanwhile, the functional properties of high-entropy alloys is vastly unexplored. In this study, we attempt to broaden the knowledge of this field, the precise formulation of this thesis would be an exploration on the possibilities of semiconducting high-entropy alloys.

A key motivation of this thesis is the ability to perform such a broad study of complex materials in light of the advances in material informatics and computational methods. In this project, we will employ Ab initio methods backed by density functional theory on top-of the line supercomputers and software. 20 years ago, at the breaking point of these methods, this study would have been significantly narrower and less detailed firstly, but secondly would have totaled ... amount of CPU hours to complete (**Calculate this number**). In the addition to the development in computational power, is also the progress of modeling materials, specifically we will apply a method called Special Quasi-random Structures (SQS) to model high-entropy alloys or generally computationally complex structures. Together with the open landscape of high-entropy alloys described above, these factors produce a relevant study in the direction of applying modern computational methods to progress the research of a novel material class and point to promising directions for future research.

In specifics, this thesis revolve around the electrical properties of high-entropy alloys, mainly the band gap as this is the key indicator for a semiconducting material and it's applicability. Semiconductors are the building blocks in many different applications in today's world, ranging

from optical and electrical devices, to renewable energy sources such as solar and thermoelectricity. Given the economic and sustainable factors concerning silicon, in addition to its role in relevant applications such as microelectronics and solar power. Silicon emerges as a natural selection to build our alloys around. Furthermore, the development and research on both high entropy alloys and metal silcides have been heavily centered around 3d transition metals. Keeping in line with the economic and environmental factors, we will continue this direction by focusing on high entropy stabilized sustainable and economic 3d metal silicides **Not happy with this writing**. Throughout the study we will analyze a great number of permutations of 3d silicides, from different initial metal silicides such as $CrSi_2$, $FeSi_2$, $MnSi_{1.75}$, Fe_2Si, each with distinct properties relating to the band gap, crystal structure and metal to silicon ratio. In addition, the permutations include numerous metal distributions and elements within the 3d-group of metals. Examples are Co, Cr, Fe, Mn, and Ni.

Given a background in high-entropy alloys, one could ask if this study is truly sensible. In the later sections we will cover the details of this field, and it quickly become clear that the materials investigated in this study does not fall under the precise definition of high-entropy alloys, nor do we intend to explore the properties and factors relating to high-entropy stabilized alloys such as the configurational entropy, phase stability and finite temperature studies. However this study is motivated from the discovery of these materials and promising properties, and venture into a more hypothetical space of materials, enabled by the computational methods available to study the potential properties of such materials. On the other hand, very recent studies **Mari, and other HEA silicide study** have experimentally synthesized high-entropy disilicides, thus in some way justifying the direction of this project.

We begin this project by reviewing key concepts of solid-state physics for readers lacking a background in materials science, and an introduction to the base 3d silicides of the experimental work. Later follows a theoretic walk-through of the relevant concepts of this thesis, these topics include high-entropy alloys, special quasi-random structures, and density functional theory. Next we shine light on the implementation of DFT in this project, and other computational details required to reproduce the results in this thesis, such as the use of the Vienna Ab Initio Simulation Package (VASP) and implementation of SQS. Finally we present the results of our study, these include the band gap and electronic properties of various structures and the success and challenges of the computational methods applied throughout the study.

Part I

Theory

Part II

Methodology and Implementation

Part III

Results and Discussion

Chapter 8

Permutations of $(CrFeMnNi)Si_2$

Up until this point we have looked in detail at the high-entropy silicide $(CrFeMnNi)Si_2$ and associated SQSs. However these structures are just the center of a larger quasi-ternary phase diagram consisting of the different possible distributions of elements Thus there exists many other compositions of this particular high-entropy silicide. In this section, we aim to expand our search of this diagram by generating SQSs of the 48 atom model slightly away from equimolar distribution of 3d elements. In table (bellow) we list the mean total energy and magnetic moment per atom with standard deviation and the enthalpy of formation of 4 compositions of the $(CrFeMnNi)Si_2$ alloy. Ideally they would differ only by one element, but the TDEP implementation insist in also reducing Nickel to stay consistent with the 48 atom supercell.

	Total energy/atom (eV)		Enthalpy of formation (eV)	Final magnetic moment (μ_B)	
$Cr_3Fe_3Mn_7Ni_3Si_{32}$	- 6.6947	0.0040	-11.9586	0.1375	0.0186
$Cr_5Fe_5Mn_3Ni_3Si_{32}$	- 6.6705	0.0030	-11.1991	0.1127	0.0223
$Cr_5Fe_3Mn_5Ni_3Si_{32}$	- 6.6852	0.0041	-10.5200	0.1375	0.0456
$Cr_3Fe_5Mn_5Ni_3Si_{32}$	- 6.6801	0.0036	-12.6426	0.0937	0.0209
$Cr_3Fe_3Mn_3Ni_7Si_{32}$	- 6.3921	0.0078	-10.9614	0.0159	0.0101

Table 8.1: Mean and standard deviation of the total energy and magnetic moment per atom, plus enthalpy of formation of the listed mean energies ($FeSi_2$).

The first result of table .. we make notice of is that the stability, as evaluated by the enthalpy of formation can be increased beyond the eqvimolar composition. This is accomplished in two distinct permutations, one with increments to manganese relative to the other TM, and the other by reduction of chromium. Moreover the two respective permutations lie on the opposite side of the magnetic scale. The large magnetic moment of the manganese rich permutation and the low magnetic moment in the chromium poor permutation is very much in line with the observations

made in the previous section. Recalling that in the magnetic moment in the eqvimolar composition was largely attributed to manganese and chromium atoms in the lattice. Thus increments to manganese or reduction of chromium would following impact the magnetic moment as in the two permutations. For this reason, additionally the permutation $Cr_5Fe_3Mn_5Ni_3Si_{32}$ where the nonmagnetic elements is reduced and the magnetic elements are increased ,is equally magnetic. We however find no direct relation between stability and magnetism as his particular permutation is the least stable. An important property of table 8.5 is that the listed values are the mean value of the observed property for 5 distinct SQSs of the same permutation. For example we notice that while the highest magnetic moment in the first permutation is associated with the most stable SQS (from total energy considerations). The least stable supercell show the highest magnetic moment in $Cr_5Fe_3Mn_5Ni_3Si_{32}$.

The respective band gaps (with PBE) can be seen in table 8.2. Compared to the previous case, we find most SQSs exhibits half-metallic character with comparative values in spin up. Alike the stability and magnetization also the band gap changes in the different directions. To some degree we find positive results of the band gap in each direction, but particularly compositions rich in manganese provide very encouraging results and compositions poor in Mn less so. In table 8.2 we note that as in previous cases, the 0 values originate from defect states in the eigenvalues and neglecting such states yield small nonzero values. In addition we list structures with defects and a finite band gap in cursive, as before these gaps disappear in the density of states. In regards to the stability we find that both the $Cr_3Fe_3Mn_7Ni_3Si_{32}$ and $Cr_3Fe_5Mn_5Ni_3Si_{32}$ compositions show the most promising properties in the utmost stable configurations.

Composition	SQS	$E_G^{\text{up, eigen}}(0.5)$	$E_G^{\text{dw, eigen}}(0.5)$	$E_G^{\text{tot, eigen}}(0.5, 0.5)$
$Cr_3Fe_3Mn_7Ni_3Si_{32}$	A	0.3390	0	0
	B	0.4745	0	0
	C	0.1342	0	0
	D	0.1950	0.0063	0.0063
	E	0.4211	0	0
Cr5Fe5Mn3Ni3Si32	A	*0.003*	0	0
	C	*0.21*	0	0
	D	0.0674	0.0413	0.0372
	E	*0.362*	0	0
Cr5Fe3Mn5Ni3Si32	**A**	0.2082	0	0
	B	0.4053	0	0
	C	0.4659	0	0
	D	0.0843	0.0121	0.0121
	E	0.3008	0	0
$Cr_3Fe_5Mn_5Ni_3Si_{32}$	A	0.3922	0	0
	C	0.1285	0	0
	D	0.2595	0.1004	0.1004
	E	0.3591	0.1003	0.0848
Cr3Fe3Mn3Ni7Si32	A	0	0	0
	B	0	0	0
	C	0	0	0
	D	0	0	0
	E	*0.04*	0	0

Table 8.2: Band gaps of various compositions of (CrFeMnNi)Si_2. Most stable SQS of a set is highlighted in bold text, band gap with defect states are listed in cursive. Some SQSs were excluded from the table due to unsuccessful calculations.

Below in figure 8.1 we plot the projected density of states around E_F of the fist four compositions of table 8.2. Note that away from the Fermi energy the projected density of states is analogous to the parent equimolar composition. The below figures is based on the most stable SQS in each permutation, as will the analysis. Hence the features of these figures can be subject to the uniqueness of that particular SQS rather than a distinct feature of the exact composition, but as stated previously the most stable configuration provide the most likely properties of the composition within the scope of this project.

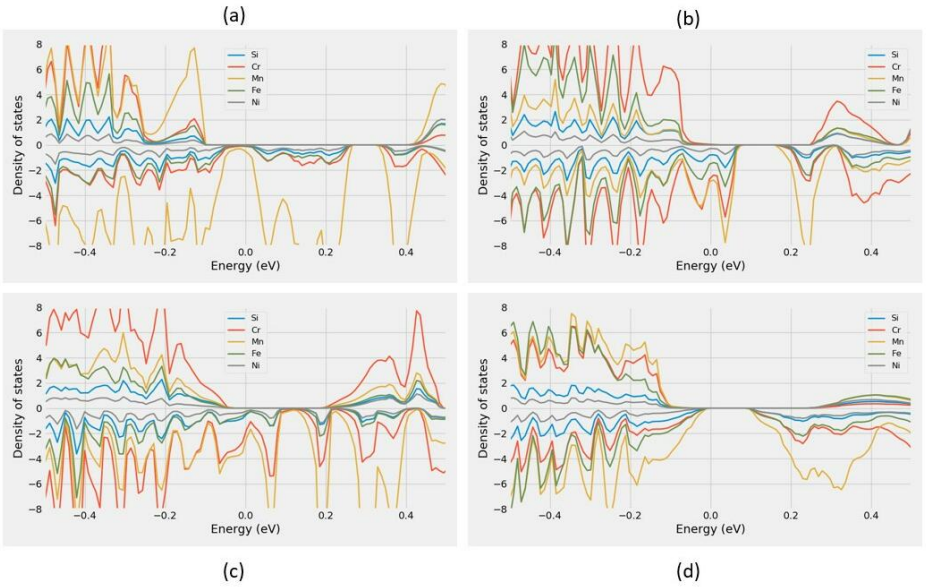

Figure 8.1: Projected density of states of (a) $Cr_3Fe_3Mn_7Ni_3Si_{32}$ (SQS B), (b) $Cr_5Fe_5Mn_3Ni_3Si_{32}$ (SQS C), (c) $Cr_5Fe_3Mn_5Ni_3Si_{32}$ (SQS A), (d) $Cr_3Fe_5Mn_5Ni_3Si_{32}$ (SQS D)

With that said, the plotted PDOSs in figure 7.1 is in good agreement with the listed values in table 7.2. $Cr_3Fe_3Mn_7Ni_3Si_{32}$ (7.1 a) and $Cr_5Fe_3Mn_5Ni_3Si_{32}$ (7.1 c) both indicate a sizable spin up band gap, further figure (7.1 d) point to a total band gap around 0.1 eV for SQS D of $Cr_3Fe_5Mn_5Ni_3Si_{32}$. On the other hand we find dissimilarity between the density of $Cr_5Fe_5Mn_3Ni_3Si_{32}$ SQS C and the eigenvalue band gap listed in table 7.2. In figure 7.1 d we find a range of forbidden energies slightly above the Fermi energy, and very small values in spin up at the Fermi energy. Similar to what we experienced in the 192 atom SQS in section 7.4, the eigenvalues report a finite band despite of defect states. Therefore the density of states is not completely zero at E_F.

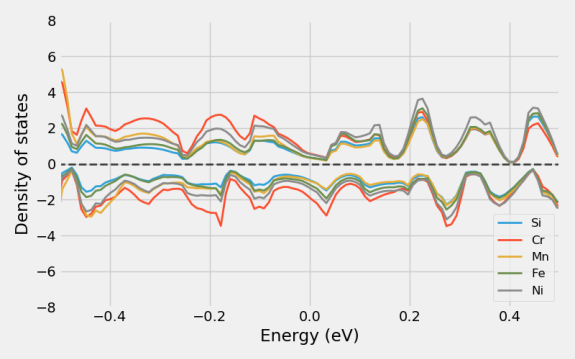

Figure 8.2: Projected density of states of $Cr_3Fe_3Mn_3Ni_7Si_{32}$ around E_F

In figure 8.6 we saw that electrons from manganese atoms in particular was a key contributor as to why the spin down channel of (CrFeMnNi)Si_2 was metallic in the stable supercell D. This is also largely the case in the permutations shown above in figure 8.12. The proportion of manganese atoms in the alloy seems to offer a very positive effect on the band gap in spin up, but is often detrimental to spin down. This is seen in figure 8.12 (a) and (c) for $Cr_3Fe_3Mn_7Ni_3Si_{32}$ and $Cr_5Fe_3Mn_5Ni_3Si_{32}$ respectively, that both contain increased amounts of manganese. By reducing the number of Mn as in (b) we still find that the Mn electrons plague the states at E_F in spin down. In analog we see from (b) and (c) that also Cr negatively impacts to the band gap especially in spin up. The sole permutation with clear evidence of a spin down gap is from the chromium poor permutation plotted in (d). Also in this structure we see that the effects of Mn around E_F is dampened in comparison to the other permutations, despite containing relatively increased amounts of Mn to the eqvimolar alloy.

An important property of these results is that because each permutation alters simultaneous elements, interpreting and relating the results to a particular alteration is challenging. For example, is the result of the $Cr_5Fe_3Mn_5Ni_3Si_{32}$ permutation a consequence of less Fe or increments to both Cr and Mn? Furthermore is the exaggerated band gap in spin up of $Cr_3Fe_3Mn_7Ni_3Si_{32}$ a product of increasing manganese or reducing the other elements. From the comparatively large gaps in spin up of $Cr_3Fe_3Mn_7Ni_3Si_{32}$ and $Cr_3Fe_5Mn_5Ni_3Si_{32}$ and the more present Cr states in spin up in the Cr rich permutations we here conclude that the band gap is related to lessening of chromium, more so than other effects. Despite of this we generally find positive results regarding most of the permutations as seen in table 8.6, the exception to this $Cr_3Fe_3Mn_3Ni_3si_{32}$. This particular permutation in opposition to the others in this section increases the proportion of Ni at the cost of the other 3d elements. The projected density of states is displayed in figure [REF]. From both this structure, but also the PDOS of $Cr_3Fe_3Mn_7Ni_3Si_{32}$ we see that reducing chromium does not always improve the band gap. It's clear that the $Cr_3Fe_5Mn_5Ni_3Si_{32}$ alloy manage to strike a balance of distribution that results in a specific interplay between the 3d elements. For this reason we more closely investigate the properties of this structure, the probability distribution of SQS D (highest stability) is

plotted bellow in figure 8.15.

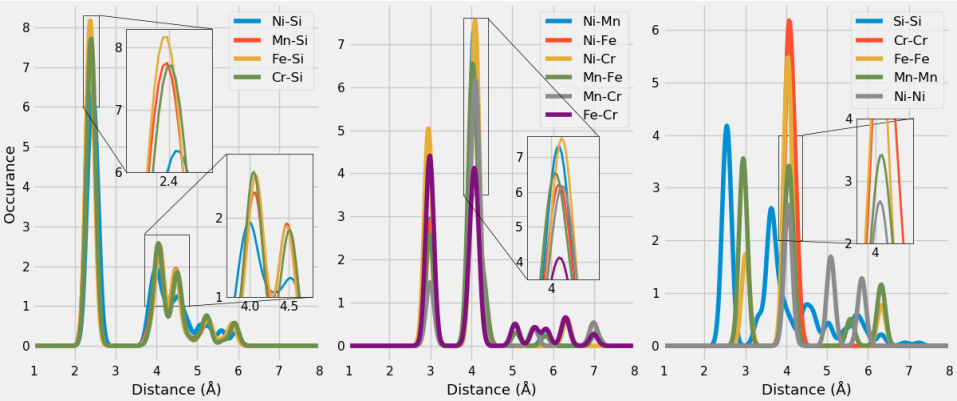

Figure 8.3: Probability distribution functions to $Cr_3Fe_5Mn_5Ni_3Si_{32}$ SQS D, **Maybe make larger**

Comment figure

Add some figures from HSE06? In this segment of the project we scarcely applied the more advanced functionals SCAN and HSE06, in part to both the uncertainties mentioned in the previous section and the computational cost of the methods. However we did perform such calculations (HSE06) to further investigate the nature of the listed semiconducting SQSs. Both the manganese rich and poor semiconductors are validated with the HSE06 functional and find wider band gaps of 0.17 eV (0.57 and 0.26 in up and down) in $Cr_3Fe_3Mn_7Ni_3Si_{32}$ SQS D, and 0.22 eV (0.77 eV in spin up) in $Cr_5Fe_5Mn_3Ni_3Si_{32}$ SQS D. On the opposite side, the very narrow band gap in $Cr_5Fe_3Mn_5Ni_3Si_{32}$ vanishes with HSE06 calculations. For the two stable semiconductors found in $Cr_3Fe_5Mn_5Ni_3Si_{32}$, simulations with the HSE06 functional resulted in a half-metal with a spin up of 0.53 eV for SQS D, and a total band-gap of 0.27 eV for E, where the spin-up gap is 0.73 eV wide . **Comparing to table 8.6 we observe that ... As for the SCAN functional ...**

Conclusion this section

Chapter 9

Different compositions and crystal structure

9.1 New compositions

In similar fashion to the previous sections, we here begin by presenting the mean and standard deviation of the total energy and magnetization of a set of SQSs corresponding to different high-entropy silicides of the $Fesi_2$ unit cell. The compositions we have tested are deliberate combinations intended to investigate both the impact of manganese by replacing the element with Co or Ti, and concepts related to HEA theory such as the atomic size effect. Furthermore Co is a very common element in many stable HEA, as seen in section .., thus we include two (3?) compositions with this element to study the impact on stability and the functional properties. The results of the aforementioned alloys can be seen bellow in table 9.1, note that all compounds contain a total of 48 atoms as before.

	Toten (eV)		Enthalpy of formation	Mag	
$Cr_4Fe_4Co_4Ni_4Si_{32}$	- 6.4655	0.0056	- 12.7536	0.0083	0.0155
$Co_4Fe_4Mn_4Ni_4Si_{32}$	- 6.4731	0.0046	- 15.0836	0.0000	0.0000
$Cr_4Fe_4Ti_4Ni_4Si_{32}$	- 6.4217	0.0087	- 7.5040	0.0305	0.0293
$Cr_4Fe_4Mn_4Ti_4Si_{32}$	-6.6994	0.0071	- 7.3060	0.1142	0.0641
$Cr_4Fe_4Mn_4Co_4Si_{32}$	-6.7687	0.0034	- 13.7796	0.1331	0.0326

Table 9.1: Summary of the total energy, enthalpy of formation and magnetization of several composistionally different SQS high-entropy alloys based on the $\beta-$ $FeSi_2$ unit cell.

Maybe discuss the std of mag and relation to energy of sqs, several cases we find large differences between SQSs. From table 9.1 we see that the stability of the relative compositions vary greatly. By introducing cobalt to the alloys, particularly at the cost of manganese result in a large positive effect on the stability, contrary replacing either manganese or nickel with titanium significantly lowers the stability. In terms of the magnetization,

the results are in line with the observations of the CFMN composition, from table 9.1 it's clear that replacing either manganese or chromium drastically reduces the magnetization of the alloys. In addition, we find indication of chromium being further significant to the magnetization than manganese as seen from the first and second compounds in table 9.1 respectively. In opposition to the study of the CFMN system we observe here a clear relation between magnetization and stability. However, we are not confident if the observed outcome is a direct consequence of the magnetization or simply a product of addition of cobalt and titanium respectively to the alloys. On the other hand, in both cases the least magnetic composition is also the most unstable, thus there is weight behind the magnetic relation to stability. **Wait for CrFeMnCoSi2 to finish**

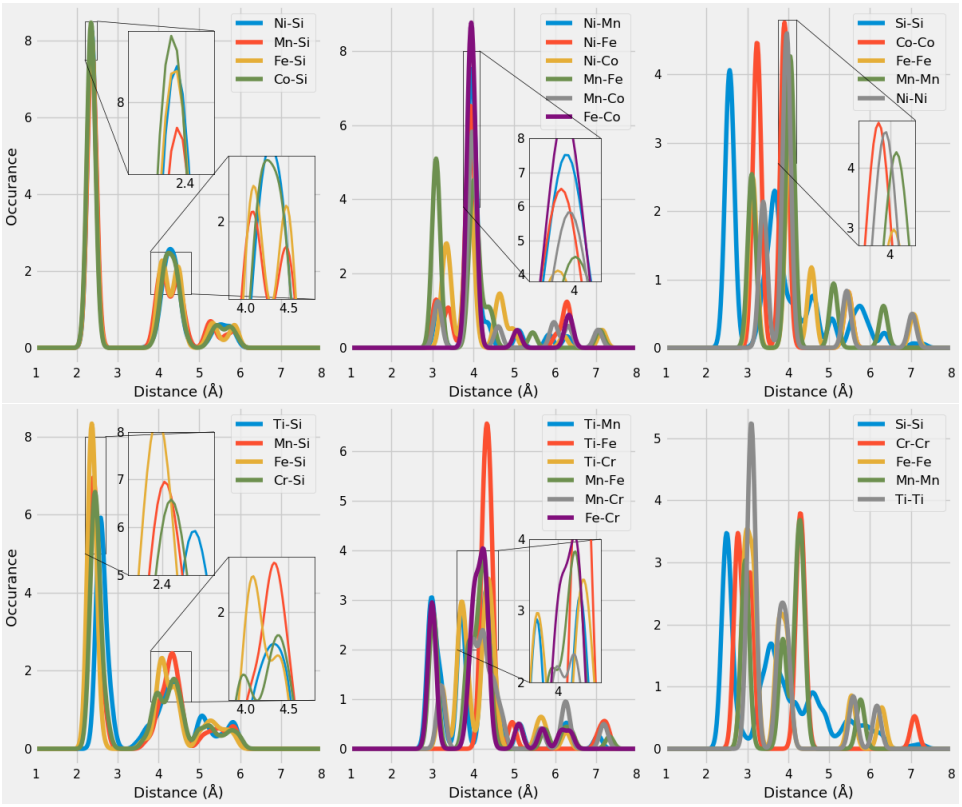

Figure 9.1: Probability distribution function of $Co_4Fe_4Mn_4Ni_4Si_{32}$ (top) and $Cr_4Fe_4M_4Ti_4Si_{32}$ (bottom)

In regards to the band gap of the compositions, we can report that a heavy majority are metals. We found no evidence of a band gap in both the CrFeCoNiSi2 and CrFeMnTiSi2 alloys across all supercells, as seen in the density of states of the two most stable SQSs of the respective compounds **Add figures**. Further also the most stable SQSs of the CrFeTiNiSi alloy point to a metal. Similarly the most stable SQSs of the CoFeMnNiSi2 alloy are clearly metals. Noteworthy of this composition however is that we find clear evidence of a narrow band gap in two SQSs (A and B). In terms of stability, these lie around the mean total energy of the set. The respective

band gaps are 0.033 eV in A and 0.0058 eV in B. **Include DOS or other figures for these results.**

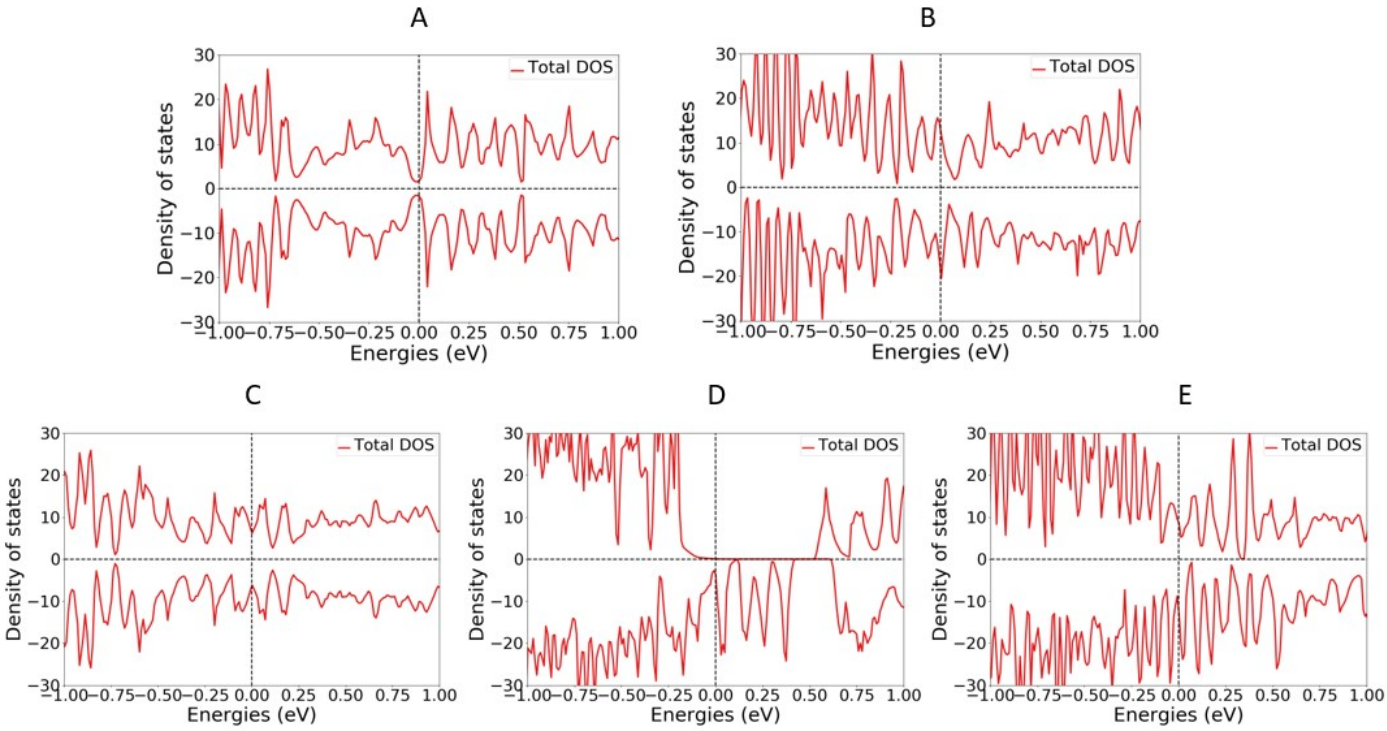

Figure 9.2: Density of states of A: $CrFeCoNiSi_2$, B: $CrFeTiNiSi_2$, C: $CoFeMnNiSi_2$, D: $CrFeMnCoSi_2$, E: $CrFeMnTiSi_2$. Calculations performed with PBE GGA.

To follow is details on the gaps in A and B, is it worth to include this? In the density of states plotted in figure .., the band gap in A is clearly visible. On the other hand the very narrow gap in B is not as apparent, as the states around Ef contain very small nonzero values. This could be related to the low resolution of 2500 points in the density of states as seen before, especially considering the size of the gap. In opposite to the CFMN calculations previous we here experience excellent cohesion between PBE and SCAN simulations on the band gap. With the meta-GGA functional the band gap of SQS A and B respective is 0.04 eV and the 0.003 eV. Moreover we find the identical gap transition with both functionals, which was not the case in previous endeavors with this functional. Additionally we also find that the HSE06 functional produce dissimilar results to previous experiences. In this scenario, the HSE06 functional fails to recognize the observed band gap of PBE and SCAN in both supercells. The greater

number of k-points in the GGA and meta-GGA calculations offer more accurate band gaps, however lesser k-points will not result in a smaller gap, only bigger. Thus the uncertainties of previous calculations of the HSE06 functional does not apply in this case. For this reason in addition to the reputation of hybrid functionals and the lack of other factors to negatively affect the validity of the result, we find it challenging to conclude on the band gap of these structures between functionals.

9.2 Crystal structures

In the discussion above we have covered in great detail the possibilites of high-entropy silicides based on the $\beta-$ $FeSi_2$ unit cell with twice as many silicon atoms to 3d elements. The primary outcome and conclsion of this research was that particularly the combination of Cr, Fe, Mn and Ni resulted in superiour properties in the light of the motivatian behind this project. The next question we wish to answer is if ihe promising results of the CFMN system be reproduced in other symetries. In this section we will implement the CFMN composistion in crystal structures based on hexagonal $CrSi_2$ ($P6_{422}$), both tetragonal and orthorombic $Mn_{16}Si_{28}$ ($P\bar{4}c2and$, $Pcca$), and trigonal Fe_2Si ($P\bar{3}m1$) where we test the CFMN system to varying metal and silicon ratioes, and crystal structures. As before, the total energy, enthalpy of formation and magnetic moment per atom can be found bellow in table ..

	Total energy	per energy	Enthalpy of formation	Mag per atom	
CrSi2	-6.4837	0.0087	-8.1205	0.0887	0.0387
MnSi	-6.6658	0.0071	-9.1848	0.0687	0.0398
Fe2Si	-7.5082	0.0107	-10.2474	0.3848	0.0588

CrSi2

From our calculations with PBE DFT we find the bulk crsi2 material to be an indirect semiconductor with a band gap of 0.33 eV, slightly bellow the listed value of 0.36 eV in materials project **cite**, suprinsingly we find a smaller gap of 0.32 eV from the SCAN functional. The compound is also nonmagnetic in agreement with materials project. Fore the bulk material we employed a 9 atom cell, with 6 silicon and 3 cr atoms, from this we generated SQSs of 72 atoms with the same ratio. **Include toten per atom for the unit cell? and figure of SQS + unit cell?**. For this given composistion and system we observe very similar results to that of the composistions discussed above, the eigenvalues of several SQSs report a small band gap, but its not apperant from neither the density of states or from the bandgap.py script of pymatgen. Additiontly, we can not repreoduce the gap with the SCAN functional, as was possible for the CFMN (fesi2) system.

MnSi

In the tetragonal configuration, the bulk material is a nonmagnetic

indirect semiconductor with a band gap of 0.76 eV acoording to our PBE calculations, and 0.78 eV from SCAN. Materials project find a band gap of 0.76 eV, in good agreement with our own PBE results. The unit cell consist of 44 total atoms, 16 manganese and 28 silicon. In the orthoromibic cell, with equal number of elements we find a band gap of 0.76 eV (0.77 ev SCAN) as well. In contrast, the CFMN alloy of both these cells produce metalic compounds. It should be noted that structures B and D in the tetragonal ssystem did not fully relax, same for D in the orthorombic cell, so these results could be inaccurate.

Fe2Si

In this cell, we drasticly alter the metal-silicon ratio, this is seen both in the band gap and magnetic properties of the material. The magnetic moment of this cell consisting of 4 iron atoms and 2 silicon atoms is 0.67, from the iron atoms. This magnetic charachter can also be observed from the discrepency between the two spin channels. In spin down we find a band gap of 0.21 eV, while there is no gap in spin up. This gap can also be seen in the density of states **Include figure**. This however is an abnormal result in regard to other experimental work and littereature on the Fe2Si **cite** $https$: $//www.sciencedirect.com/science/article/pii/S0925838816329796?casa_token = g9DRpU9IClcAAAAA : 6Gd12A4Kh9J2igUWMVwHN8OSIKzD27VACA052FNsSAWhRY6PE$ Our results are subject to errors, particularly we note that the eigenvalues used to calculate the gap contain nonphysical values in the spin down channel. However, the gap is evident in the density of states thus we include the result in this report, but acknowlendge the uncertainties revolving the value.

From this unit cell we generate 54 atom SQSs. From table .. we see that the magnetic nature remains, producing the overall highest magnetic moment of all studied supercells, which is not a surprising result considering the 3d metal to silicon ratio. **More on magnetic and total energy.** The magnetism can also be seen in the difference between the two spin channels, the bands where the occupancy transistion from 1 to 0, ie occupied to not occupied is very different. In the most magnetic supercell D, we saw a distance of 22 bands between the spin down transistion and spin down transistion. Most supercells are metals from our PBE calculations. B and D show a very small gap of around 0.01 eV in one spin channel. In E we find a very narrow gap semiconductor with a total gap of 0.002 eV. This gap is surrounded by the same uncertainties as discussed previosly.

Part IV

Conclusion

Write conclusion here